RSC Advances

PAPER

View Article Online
View Journal | View Issue

Cite this: *RSC Adv.*, 2020, **10**, 3832

Single crystals of mixed Br/Cl and Sn-doped formamidinium lead halide perovskites *via* inverse temperature crystallization†

Michael Ng [ab] and Jonathan E. Halpert *[ab]

Hybrid organic–inorganic perovskite mixed halides of $FAPbBr_{3-x}Cl_x$ and doped $FAPb_{1-x}Sn_xBr_3$ were synthesized using a generalized inverse temperature crystallization (ITC) method. With an appropriate choice of solvents and crystallization temperatures we show that large millimeter sized single crystals of these hybrid perovskites can be grown in a matter of hours to days using ITC. The structural and optical properties of these single crystals were characterized systematically. The mixed metal and mixed halide perovskites displayed a compositional bandgap tuneability in the region of 2.05 eV to 2.57 eV. The electrical properties of the perovskite single crystals were determined using a space-charge limited current (SCLC) method. The trap density determined from SCLC was between 10^9 and 10^{11} cm^{-3} for all perovskites which is exceptionally low. The mobility was found to increase by one order of magnitude on the addition of only 3% Sn for $FAPb_{1-x}Sn_xBr_3$ based perovskites which shows promise for enhancing the electrical properties. This demonstrates the generalizability of the ITC method to grow large high-quality perovskite single crystals with enhanced optical and electrical properties. In addition, it was observed for $FAPbBr_{3-x}Cl_x$ based perovskites that initially degraded surfaces with suppressed PL emission could be repaired by using an anti-solvent treatment re-enabling the PL emission. Other perovskite compounds did not display any degraded surfaces and exhibited excellent stability in ambient conditions.

Received 7th August 2019
Accepted 13th January 2020

DOI: 10.1039/d0ra00060d

rsc.li/rsc-advances

Introduction

In recent years, organic–inorganic halide perovskites (AMX_3) have been the focus of intense research due to their remarkable optical and electrical properties.[1–6] Recently, single crystal organic–inorganic halide perovskites have been shown to exhibit significantly longer diffusion lengths, higher mobilities and lower trap densities than polycrystalline thin films.[7–9] These enhanced properties make single crystals attractive for further improving optoelectronic device performance. Typically single crystals have been grown using cooling induced precipitation (CIP),[10,11] seeded solution growth,[3] or vapour-assisted crystallisation,[8] however these methods typically take weeks to months to prepare high quality crystalline samples.

Inverse temperature crystallisation (ITC) is method which takes advantage of the observed retrograde solubility of perovskites, allowing rapid growth of high-quality, millimetre-sized perovskites in a matter of days.[7,12,13] Based on the ITC approach single crystal materials of $MAPbX_3$ (MA = methylammonium and X = halide),[7,13,14] $FAPbX_3$ (FA = formamidinium),[12,15,16] $CsPbBr_3$,[17–19] $MAPbBr_{3-x}Cl_x$,[20–23] $MAPbBr_{3-x}I_x$[21,23–26] and heterovalent doped $MAPbBr_3$ [27] and $MAPbCl_3$ [28] have been reported. It has been shown that substitution of MA for FA can lead to improved stability in solar cells[29] and enhanced charge transport properties in thin films[30,31] and single crystals[16] compared to their $MAPbX_3$ counterparts. However, formamidinium based mixed single crystals have yet to be reported. Here we report the successful synthesis of large, millimetre-sized, single crystal perovskites containing mixed halides of $FAPbBr_{3-x}Cl_x$ and doped metals of $FAPb_{1-x}Sn_xBr_3$ with low trap densities using ITC. The incorporation of both mixed halides and doped metals into the single crystal perovskites permits tuning of the band gap across the visible spectrum and alters its electrical properties. While investigating air stability of these materials, $FAPbBr_{3-x}Cl_x$ based single crystals were found to exhibit a degraded surface species that could be repaired using an anti-solvent treatment (see ESI†).

Experimental

Chemicals and reagents

Lead bromide ($PbBr_2$, ≥98%), lead chloride ($PbCl_2$, 98%), *N*,*N*-dimethylformamide (DMF, anhydrous, 99.8%), dimethyl sulfoxide (DMSO, anhydrous, ≥99.9%), tin(II) bromide ($SnBr_2$) and methylamine solution (33 wt% in absolute ethanol) were

[a]*Department of Chemistry, Hong Kong University of Science and Technology, Clear Water Bay Rd, Kowloon, Hong Kong SAR. E-mail: jhalpert@ust.hk*

[b]*MacDiarmid Institute for Advanced Materials and Nanotechnology, School of Chemical and Physical Sciences, Victoria University of Wellington, Gate 7 Kelburn Parade, Wellington, New Zealand*

† Electronic supplementary information (ESI) available. See DOI: 10.1039/d0ra00060d

purchased from Sigma-Aldrich. Methylammonium bromide (MABr) and formamidinium bromide (FABr) were purchased from Dyesol Limited. γ-Butyrolactone (GBL, 99+%) was purchased from Acros Organics. All precursors were used as received without any further purification.

Synthesis

In general solutions were prepared by dissolving AX and MX_2 precursors in a suitable solvent (DMF/DMSO/GBL). After the precursors have dissolved the solution is filtered using a 0.22 μm PTFE hydrophilic filter. 2 mL of the solution is than placed into a glass vial with a 21G needle and heated in oil bath. Further details on specific temperatures, reaction conditions and initial precursor concentrations can be found in the ESI.†

Measurement and characterization

Powder X-ray diffraction was performed on a Panalytical X'Pert Pro diffractometer using a Cu-Kα radiation. The steady state absorption was carried out on a Varian Cary 50 UV-vis spectrophotometer. Photoluminescence emission and decay were carried out on a Horiba Jobin Yvon Fluorolog/Fluorohub setup, a xenon lamp was used as the source for PL emission and a 265 nm NanoLed was used as the source for TCSPC. EDS elemental analysis was carried out using a Jeol JSM-6610 SEM. *I–V* characteristics were carried out in the dark under ambient conditions with an Agilent 4156C Precision Semiconductor Parameter Analyser.

Results and discussion

Synthesis and characterization

Unlike $MAPbBr_{3-x}Cl_x$ there are no reports of $FAPbBr_{3-x}Cl_x$ single crystals as far as we are aware. In order to grow large $FAPbBr_{3-x}Cl_x$ single crystals, a 1 : 1 v/v mixture of DMF–GBL can still be used similar to pure $FAPbBr_3$.[12] However, due to the lower solubility of $PbCl_2$ in DMF, the concentration and crystallisation temperature must be decreased with the increasing $PbCl_2$ inclusion to optimise the crystal growth. Using the optimised reaction conditions (Table S1, ESI†), large single crystals of $FAPbBr_{3-x}Cl_x$ were grown in just a few days. Photographs of the single crystals with a total synthesis time of 20 hours and a total synthesis time > 48 hours can be found in Fig. 1A and B, respectively. It was observed that for reactions with a total synthesis time of 20 hours the resulting single crystals were orange, yellow and pale yellow for $FAPbBr_{2.69}Cl_{0.31}$, $FAPbBr_{2.23}Cl_{0.77}$ and $FAPbBr_{1.33}Cl_{1.67}$ respectively. These results are similar to those observed for $MAPbBr_{3-x}Cl_x$ based perovskites (Fig. S2, ESI†). However, if the total synthesis times were increased to >48 hours then the single crystals were observed to be very dark orange. This suggests that an increase in the synthesis time under ambient conditions can lead to degradation of $FAPbBr_{3-x}Cl_x$. Powder XRD spectra were collected for samples with a total synthesis time of 20 hours and are shown in Fig. 1D and the corresponding lattice constants are shown in Table 1. For $FAPbBr_{3-x}Cl_x$ perovskites the diffraction peaks shift to higher angles with increasing Cl content thus indicating

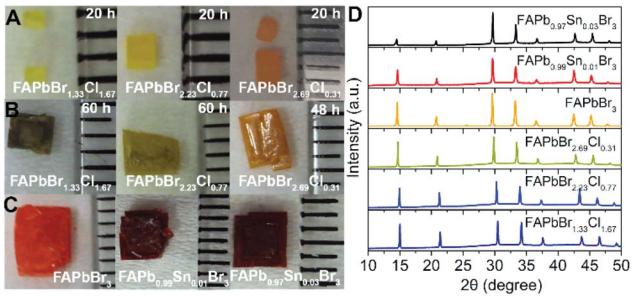

Fig. 1 Photographs of $FAPbBr_{3-x}Cl_x$ (A) based perovskites with a total synthesis time of 20 hours and (B) with a total synthesis time > 48 hours showing a degradation of the surface with increased synthesis time. (C) Photographs of $FAPb_{1-x}Sn_xBr_3$ based perovskites. (D) Powder XRD spectra of FA based perovskites with different halide and metal compositions.

a decrease in the lattice constant due to the inclusion of the smaller Cl atomic radius. The powder XRD spectra were also collected for the degraded samples (Fig. S3, ESI†). The powder XRD spectra showed no difference between the samples with the same nominal Cl inclusion irrespective of the total synthesis time. Furthermore, upon grinding the samples for XRD the resulting powders were observed to have a similar colour regardless of the total synthesis time (Fig. S4, ESI†). This suggests that the increased synthesis time has resulted in the formation of degraded surface species, see the ESI† for a more detailed discussion on the degraded surface and how it can be repaired using a simple anti-solvent treatment. Energy dispersive X-ray spectroscopy (EDS) was used to identify the actual composition of the mixed halides and mixed metals present in the single crystals. The elemental compositions are summarised in Table 1. We can see that the nominal Cl inclusion is close to that determined using EDS. This also resembles the observations for $MAPbBr_{3-x}Cl_x$ analogues grown using ITC (Table S2, ESI†), where no preferential incorporation of Br or Cl is observed. Single crystals of $MAPb_{1-x}Sn_xBr_3$ have been recently reported *via* the TSSG method,[32] motivated by this report we also attempted to synthesize mixed Pb/Sn single crystals using ITC. Using DMF–GBL (1 : 1 v/v) as a solvent, perovskites of $FAPb_{1-x}Sn_xBr_3$ were successfully achieved by substituting an equal molar ratio of $PbBr_2$ for $SnBr_2$ and using and inert atmosphere to prevent Sn oxidation. Specific reaction conditions can be found in the ESI.† Photographs of the $FAPb_{1-x}Sn_xBr_3$ perovskites are shown in Fig. 1C. We can see that with increasing Sn inclusion the crystals appear from orange for pure Pb, to dark red for mixed metals (1% and 3% of Sn). The powder XRD spectra are shown in Fig. 1D. The diffraction peaks for $FAPb_{1-x}Sn_xBr_3$ based perovskites are shifted to slightly higher angles with increasing Sn inclusion resulting in a smaller lattice constant as summarized in Table 1. The actual composition of Sn in the doped metal perovskites are shown in Table 1. We can see that the actual percentage of Sn incorporated into the perovskite is only between 1–3%. This shows a preferential incorporation of Pb relative to Sn in the $FAPb_{1-x}Sn_xBr_3$ based perovskites, only allowing dopant level

Table 1 Summary of elemental composition determined from EDS and lattice constants determined from XRD for $FAPbBr_{3-x}Cl_x$ and $FAPb_{1-x}Sn_xBr_3$ single crystals

Samples	Lattice constant (Å)	Nominal Cl or Sn inclusion (in solution)	Actual Cl or Sn inclusion (*via* EDS)
$FAPbBr_3$	6.03	—	—
$FAPbBr_{2.69}Cl_{0.31}$ [a]	5.99	16.7% (Cl)	10.3% (Cl)
$FAPbBr_{2.23}Cl_{0.77}$ [a]	5.90	33.3% (Cl)	25.6% (Cl)
$FAPbBr_{1.33}Cl_{1.67}$ [b]	5.86	50.0% (Cl)	55.7% (Cl)
$FAPb_{0.99}Sn_{0.01}Br_3$	6.02	25.0% (Sn)	1.0% (Sn)
$FAPb_{0.97}Sn_{0.03}Br_3$	5.98	50.0% (Sn)	3.0% (Sn)

[a] Perovskites placed in anti-solvent (dichloromethane) for 4 months to repair the crystal surface. [b] Perovskites placed in anti-solvent (chloroform) for 1 month to repair the crystal surface.

incorporation of Sn to be achieved using ITC. Similar percent level dopants of Sn are also observed for MA analogues that we synthesized using ITC (Table S2, ESI†), and as such this method appears to be generally less useful than TSSG for preparing mixed metal single crystals.

Optical characterization

The absorption and PL spectra for $FAPbBr_{3-x}Cl_x$ single crystals are shown in Fig. 2A. The absorption edges are blue-shifted with increasing Cl content and show a similar trend to the photographs. The absorption edge for perovskites with different synthesis times also appear blue shifted, suggesting that the observed differences in the photographs of the single crystals are indeed a surface effect which is discussed in more detail in the ESI.† Similar to $MAPbBr_{3-x}Cl_x$ based perovskites the PL emissions are blue-shifted but otherwise show similar trends to the absorption spectra with increasing Cl content (Fig. S7, ESI†). The blue shifted (see ESI† for more detail) PL peak is similar to

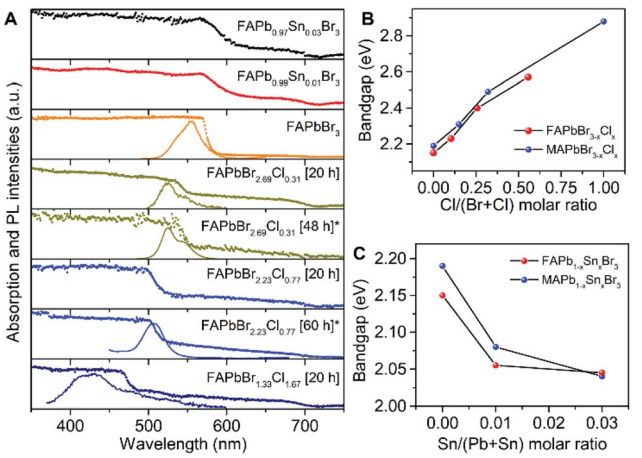

Fig. 2 Absorption and PL spectra for (A) FA based perovskites with mixed halides or mixed metals. *Absorption and PL spectra collected for samples with degraded surface (total synthesis time > 48 hours). Band gap of (B) mixed Br/Cl perovskites and (C) mixed Pb/Sn perovskites extrapolated from Tauc plots.

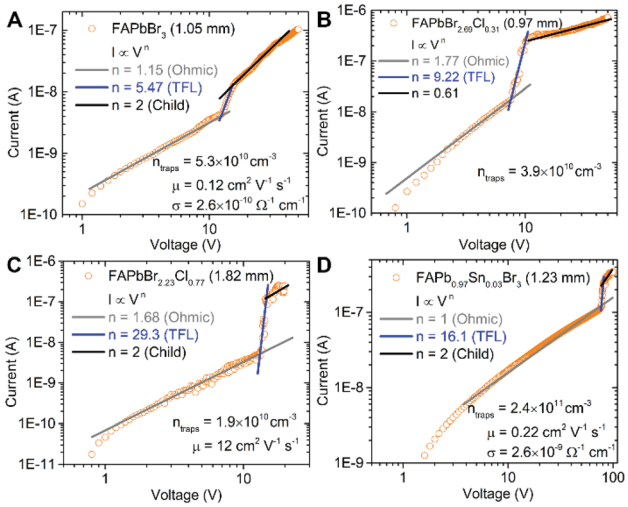

Fig. 3 *I–V* curves of (A) $FAPbBr_3$, (B) $FAPbBr_{2.69}Cl_{0.31}$, (C) $FAPBr_{2.23}Cl_{0.77}$, and (D) $FAPb_{0.97}Sn_{0.03}Br_3$ perovskite single crystals with regions corresponding to SCLC theory. The crystal thickness is givens in the parenthesis and the conductivities are calculated from the ohmic regime, the trap densities are calculated from the TFL and the mobilities are determined from the Child's regime.

other perovskite single crystals grown using CIP.[11] With this in mind, Tauc plots (Fig. S8, ESI†) are used to extract an estimate of the band gaps. The estimated band gaps for mixed Br/Cl single crystals are shown in Fig. 2B. We can see a rough linear trend with increasing Cl content. In general, the $FAPbBr_{3-x}Cl_x$ perovskites show a slight red shift compared to their $MAPbBr_{3-x}Cl_x$ analogues.

UV-vis absorption spectra are shown in Fig. 2A for the tin-doped $FAPb_{1-x}Sn_xBr_3$ single crystals. We can see that the incorporation of only 1–3% Sn results in a much broader absorption edge which is red-shifted relative to pure $FAPbBr_3$. We observe a similar trend for MA analogues as shown in Fig. 2C. No PL emission was observed for the doped Sn single crystals, ostensibly due to an increased number of trap states (relative to pure $FAPbBr_3$, see Fig. 3) causing non-radiative recombination.

Electrical characterization

The current–voltage (*I–V*) properties were measured using a sandwich type device (Au/perovskite/Au) structure with two Au (100 nm) electrodes. Under an applied bias the dark current should follow the space charge limited current model (SCLC),[33,34] which displays three distinct regimes. It should be noted that not all the single crystal perovskite materials exhibited all three distinct regions, as is shown in Fig. 3. Nevertheless the SCLC method has been consistently used to measure single crystal properties in the literature, despite some limitations.[3,7,8,13–16,19,35] See the ESI† for a more detailed discussion on SCLC theory and extracting electrical properties.

Conductivities are largely comparable with literature with the exception of $FAPbBr_3$, which has a conductivity of 2.0×10^{-10} S cm^{-1}, about two orders of magnitude lower than previous reports on other FA single crystals.[13,16] This may be due to

degradation of the perovskite surfaces upon exposure to humid conditions. The addition of 1–3% Sn in $FAPb_{1-x}Sn_xBr_3$ has resulted in up to a 2 order of magnitude increase in the conductivity, and this trend is also observed for $MAPb_{1-x}Sn_xBr_3$ analogues prepared by ITC (Fig. S10, ESI†). In general, the trap density of our single crystal perovskites is between 10^9–10^{11} cm^{-3} which is significantly lower than their thin film counterparts and comparable to previous reports on perovskite single crystals (Fig. S11 and Table S4, ESI†).[3,7,8,13–16,19,35,36] For $FAPb_{1-x}Sn_xBr_3$ based perovskites the inclusion of only several percent of Sn has resulted in an increase in trap density by 1 order of magnitude and $MAPb_{1-x}Sn_xBr_3$ perovskites also exhibit similar trends (Fig. S10, ESI†). The hole mobilities for $FAPbBr_3$ were found to be 0.12 cm^2 V^{-1} s^{-1} which appears to be lower than that determined previously,[16] perhaps in part related to the observed degradation at the surface of these FA based perovskites. In the case of $FAPbBr_{2.23}Cl_{0.77}$ the mobility is 12 cm^2 V^{-1} s^{-1} which is two orders of magnitude higher than pure $FAPbBr_3$. This suggests that Cl inclusion may be a useful approach to enhance the mobility. In the case of $FAPb_{0.5}Sn_{0.5}Br_3$, we find a mobility of 0.22 cm^2 V^{-1} s^{-1}. This is a moderate increase compared to MA based analogues which exhibits a two order of magnitude increase for 3% Sn inclusion (Fig. S10, ESI†).

Conclusion

In summary, the ITC method was successfully generalized to synthesize large single crystals of $FAPbBr_{3-x}Cl_x$ and doped $FAPb_{1-x}Sn_xBr_3$ mixed perovskites with only minor variations in preparation technique. Structural and optical characterizations were carried out to obtain a highly tuneable bandgap for mixed halide and doped metal single crystal perovskites grown using ITC. In addition, $FAPbBr_{3-x}Cl_x$ single crystals with degraded surfaces were successfully repaired using a simple anti-solvent treatment, leading to enhanced PL emissions. The conductivity was found to increase with the inclusion of only 1–3% Sn for $FAPb_{1-x}Sn_xBr_3$ based perovskites, similar to their MA analogues. Overall the trap density for our single crystals perovskites is between 10^9–10^{11} cm^{-3} which is exceptionally low. The mobility of the mixed halide and doped metal perovskites increased upon both Cl and Sn inclusion, suggesting that Cl and Sn inclusion could lead to an enhancement in the charge transport properties for FA based single crystals. This demonstrates that ITC can be generalized to grow a wide variety of high quality formamidinium perovskite single crystals in a matter of days.

Conflicts of interest

There are no conflicts to declare.

Acknowledgements

The authors acknowledge funding from HKUST *via* fund R9398 and *via* the School of Science (SSCI) fund IGN17SC05. Authors also recognize the MacDiarmid Institute for Advanced Materials and Nanotechnology, as well the Royal Society of New Zealand *via* grant E2646/3416. JEH acknowledges funding *via* a Rutherford Discovery Fellowship, E2675/2990.

Notes and references

1 G. C. Xing, N. Mathews, S. Y. Sun, S. S. Lim, Y. M. Lam, M. Gratzel, S. Mhaisalkar and T. C. Sum, *Science*, 2013, **342**, 344–347.
2 S. D. Stranks, G. E. Eperon, G. Grancini, C. Menelaou, M. J. P. Alcocer, T. Leijtens, L. M. Herz, A. Petrozza and H. J. Snaith, *Science*, 2013, **342**, 341–344.
3 Q. F. Dong, Y. J. Fang, Y. C. Shao, P. Mulligan, J. Qiu, L. Cao and J. S. Huang, *Science*, 2015, **347**, 967–970.
4 C. C. Stoumpos, C. D. Malliakas and M. G. Kanatzidis, *Inorg. Chem.*, 2013, **52**, 9019–9038.
5 C. S. Ponseca, T. J. Savenije, M. Abdellah, K. B. Zheng, A. Yartsev, T. Pascher, T. Harlang, P. Chabera, T. Pullerits, A. Stepanov, J. P. Wolf and V. Sundstrom, *J. Am. Chem. Soc.*, 2014, **136**, 5189–5192.
6 S. De Wolf, J. Holovsky, S. J. Moon, P. Loper, B. Niesen, M. Ledinsky, F. J. Haug, J. H. Yum and C. Ballif, *J. Phys. Chem. Lett.*, 2014, **5**, 1035–1039.
7 M. I. Saidaminov, A. L. Abdelhady, B. Murali, E. Alarousu, V. M. Burlakov, W. Peng, I. Dursun, L. F. Wang, Y. He, G. Maculan, A. Goriely, T. Wu, O. F. Mohammed and O. M. Bakr, *Nat. Commun.*, 2015, **6**, 7586.
8 D. Shi, V. Adinolfi, R. Comin, M. J. Yuan, E. Alarousu, A. Buin, Y. Chen, S. Hoogland, A. Rothenberger, K. Katsiev, Y. Losovyj, X. Zhang, P. A. Dowben, O. F. Mohammed, E. H. Sargent and O. M. Bakr, *Science*, 2015, **347**, 519–522.
9 Y. H. Shao, Z. G. Xiao, C. Bi, Y. B. Yuan and J. S. Huang, *Nat. Commun.*, 2014, **5**, 5784.
10 Y. Y. Dang, Y. Liu, Y. X. Sun, D. S. Yuan, X. L. Liu, W. Q. Lu, G. F. Liu, H. B. Xia and X. T. Tao, *CrystEngComm*, 2015, **17**, 665–670.
11 Y. J. Fang, Q. F. Dong, Y. C. Shao, Y. B. Yuan and J. S. Huang, *Nat. Photonics*, 2015, **9**, 679–686.
12 M. I. Saidaminov, A. L. Abdelhady, G. Maculan and O. M. Bakr, *Chem. Commun.*, 2015, **51**, 17658–17661.
13 G. Maculan, A. D. Sheikh, A. L. Abdelhady, M. I. Saidaminov, M. A. Hague, B. Murali, E. Alarousu, O. F. Mohammed, T. Wu and O. M. Bakr, *J. Phys. Chem. Lett.*, 2015, **6**, 3781–3786.
14 Y. C. Liu, Z. Yang, D. Cui, X. D. Ren, J. K. Sun, X. J. Liu, J. R. Zhang, Q. B. Wei, H. B. Fan, F. Y. Yu, X. Zhang, C. M. Zhao and S. Z. Liu, *Adv. Mater.*, 2015, **27**, 5176–5183.
15 Q. F. Han, S. H. Bae, P. Y. Sun, Y. T. Hsieh, Y. Yang, Y. S. Rim, H. X. Zhao, Q. Chen, W. Z. Shi, G. Li and Y. Yang, *Adv. Mater.*, 2016, **28**, 2253–2258.
16 A. A. Zhumekenov, M. I. Saidaminov, M. A. Haque, E. Alarousu, S. P. Sarmah, B. Murali, I. Dursun, X. H. Miao, A. L. Abdelhady, T. Wu, O. F. Mohammed and O. M. Bakr, *ACS Energy Lett.*, 2016, **1**, 32–37.
17 P. K. Nayak, D. T. Moore, B. Wenger, S. Nayak, A. A. Haghighirad, A. Fineberg, N. K. Noel, O. G. Reid, G. Rumbles, P. Kukura, K. A. Vincent and H. J. Snaith, *Nat. Commun.*, 2016, **8**, 13303.

18 Y. Rakita, N. Kedem, S. Gupta, A. Sadhanala, V. Kalchenko, M. L. Bohm, M. Kulbak, R. H. Friend, D. Cahen and G. Hodes, *Cryst. Growth Des.*, 2016, **16**, 5717–5725.
19 M. I. Saidaminov, M. A. Haque, J. Almutlaq, S. Sarmah, X. H. Miao, R. Begum, A. A. Zhumekenov, I. Dursun, N. Cho, B. Murali, O. F. Mohammed, T. Wu and O. M. Bakr, *Adv. Opt. Mater.*, 2017, **5**, 1600704.
20 T. Y. Zhang, M. J. Yang, E. E. Benson, Z. J. Li, J. van de Lagemaat, J. M. Luther, Y. F. Yan, K. Zhu and Y. X. Zhao, *Chem. Commun.*, 2015, **51**, 7820–7823.
21 Y. C. Liu, X. D. Ren, J. Zhang, Z. Yang, D. Yang, F. Y. Yu, J. K. Sun, C. M. Zhao, Z. Yao, B. Wang, Q. B. Wei, F. W. Xiao, H. B. Fan, H. Deng, L. P. Deng and S. Z. Liu, *Sci. China: Chem.*, 2017, **60**, 1367–1376.
22 H. T. Wei, D. DeSantis, W. Wei, Y. H. Deng, D. Y. Guo, T. J. Savenije, L. Cao and J. S. Huang, *Nat. Mater.*, 2017, **16**, 826–833.
23 W. F. Wang, J. Su, L. Zhang, Y. Lei, D. Wang, D. Lu and Y. Bai, *CrystEngComm*, 2018, **20**, 1635–1643.
24 Y. X. Zhang, Y. C. Liu, Y. J. Li, Z. Yang and S. Z. Liu, *J. Mater. Chem. C*, 2016, **4**, 9172–9178.
25 H. R. Byun, D. Y. Park, H. M. Oh, G. Namkoong and M. S. Jeong, *ACS Photonics*, 2017, **4**, 2813–2820.
26 F. Y. Zhang, B. Yang, X. Mao, R. X. Yang, L. Jiang, Y. J. Li, J. Xiong, Y. Yang, R. X. He, W. Q. Deng and K. L. Han, *ACS Appl. Mater. Interfaces*, 2017, **9**, 14827–14832.
27 A. L. Abdelhady, M. I. Saidaminov, B. Murali, V. Adinolfi, O. Voznyy, K. Katsiev, E. Alarousu, R. Comin, I. Dursun, L. Sinatra, E. H. Sargent, O. F. Mohammed and O. M. Bakr, *J. Phys. Chem. Lett.*, 2016, **7**, 295–301.
28 Z. Zhang, L. X. Ren, H. Yan, S. J. Guo, S. H. Wang, M. Wang and K. X. Jin, *J. Phys. Chem. C*, 2017, **121**, 17436–17441.
29 G. E. Eperon, S. D. Stranks, C. Menelaou, M. B. Johnston, L. M. Herz and H. J. Snaith, *Energy Environ. Sci.*, 2014, **7**, 982–988.
30 F. C. Hanusch, E. Wiesenmayer, E. Mankel, A. Binek, P. Angloher, C. Fraunhofer, N. Giesbrecht, J. M. Feckl, W. Jaegermann, D. Johrendt, T. Bein and P. Docampo, *J. Phys. Chem. Lett.*, 2014, **5**, 2791–2795.
31 W. Rehman, R. L. Milot, G. E. Eperon, C. Wehrenfennig, J. L. Boland, H. J. Snaith, M. B. Johnston and L. M. Herz, *Adv. Mater.*, 2015, **27**, 7938–7944.
32 D. X. Ju, Y. Y. Dang, Z. L. Zhu, H. B. Liu, C. C. Chueh, X. S. Li, L. Wang, X. B. Hu, A. K. Y. Jen and X. T. Tao, *Chem. Mater.*, 2018, **30**, 1556–1565.
33 A. Rose, *Phys. Rev.*, 1955, **97**, 1538–1544.
34 R. H. Bube, *J. Appl. Phys.*, 1962, **33**, 1733–1737.
35 H. S. Rao, W. G. Li, B. X. Chen, D. B. Kuang and C. Y. Su, *Adv. Mater.*, 2017, **29**, 1602639.
36 B. Wenger, P. K. Nayak, X. M. Wen, S. V. Kesava, N. K. Noel and H. J. Snaith, *Nat. Commun.*, 2017, **5**, 590.